Pixel Purity Index Applied to the Mapping of Degraded Soils by the Presence of Cangahuas in the Ilaló Volcano, Ecuador

Iván Palacios [a,*], Dennis Ushiña [a], David Carrera [a,b]

[a] *Department of Earth and Construction Sciences, University of the Armed Forces ESPE, Av. Gral. Rumiñahui, Sangolquí, 170501, Ecuador*
[b] *Faculty of Geology, Mines, Petroleum and Environmental Engineering, Central University of Ecuador, Quito, 170521, Ecuador*
*Corresponding author: *[*ifpalacios@espe.edu.ec*](mailto:ifpalacios@espe.edu.ec)

Abstract— **Soil degradation is a severe problem in the northern region of Ecuador. Due to deforestation, expansion of the agricultural frontier, and poor tillage practices, the outcrop of cangahuas further aggravates. Remote Sensing allows mapping this type of subsoil, which is often related to eroded areas; the spatial resolution of free multispectral images contains more than one coverage. This means that techniques to discern the pure spectral signature of the object of interest are required. Pixel Purity Index (PPI) is an endmember extraction algorithm capable of selecting the pure pixel and classifying it better than object-oriented techniques. The study's objective was to map soils with outcrops of cangahua, by PPI applied to Landsat 8 images in Ilaló volcano and later performed a physicochemical characterization to know the magnitude of the soil degradation in the mapped areas. We used two models with PPI: SAM and LSU; both were compared with classifications based on three vegetation indexes. LSU obtained the best result (91.2% accuracy and 0.81 Kappa coefficient). The mapped cangahua was approximately 806.85 ha. The soil had an average porosity of 45%, a relative density of 2.271 g/cm3, low concentrations of nitrates, phosphates, and sulfates, electrical conductivity <500 µS/cm, and alkaline pH, this means there is soil degradation. The PPI method had good accuracy and was achieved in identifying cangahua outcrops, which demonstrated its potentiality in mapping land cover.**

Keywords— **Endmembers; remote sensing; physicochemical characterization.**

I. INTRODUCTION

The development of instruments for Earth observation, such as satellites, has made it possible to obtain more accurate information about the topographic reality of the planet. Remote Sensing allows studying a geographic object using data represented in a satellite image [1]. This technique is very useful for monitoring changes in land cover [2]. It has been extensively studied in topics such as plant stress detection [3]; seed chlorophyll [4]; vegetation index calculation [5]; water body discrimination [6]; urban sprawl [7]; and other applications. However, in most free access multispectral images, owing to the spatial resolution that they present (30 meters on the Landsat satellite), the information contained in the pixel often presents noise [8], that leads to mistakes in common object-oriented classification techniques (supervised and unsupervised) [9]. A mixed pixel is an element that represents an area with more than one coverage [10]. If an image of the Landsat satellites is being considered, it would be logical to infer that there will be two or more coverages in the same pixel due to its spatial resolution, so methodologies capable of discerning the purity of the data representing the object to be studied are required.

In remote sensors, selecting extreme members is essential for the correct mapping of existing surfaces in a study area [11]. Endmember means the pure signature idealized for a class [12]. There are several algorithms for obtaining extreme members of an image, such as N-finder (N-FINDR) algorithm, Iterative Error Analysis (IEA), Automated morphological Endmember Extraction (AMEE) algorithm, Minimum Volume Transform, Convex Geometry, and Pixel Purity Index (PPI), the latter, is widely used due to its remarkable ability to extract endmembers [13].

In the case of Ecuador, several works have dealt with the identification of land covers using commonly supervised or unsupervised classification techniques [14], [15], but very few have used PPI to identify areas with soil degradations. In studies such as the ones developed by Jimenez *et al.* [14] to map cangahua in Ecuador using Remote Sensing, although specialized software and supplies such as satellite images and orthophotos are used, the classification of soils is done by the

interpretation of the geomorphological features. Pixel sorting methods are not widely applied in these cases, even when they could provide relevant information by interpreting land area covers; this information can allow us to identify areas affected by erosion and the causes related to this process.

The loss of soil resources is a worrying reality in the central region of Ecuador. Every year, the situation worsens due to the agricultural frontier's advance, poor planting practices, and indiscriminate logging. Erosion is aggravated by losing the productive topsoil layer, which gives way to the outcrop of cangahuas, a typical soil in the Inter-Andean region of Ecuador [16].

The objectives of this study are as follows:

- Mapping the soils with the presence of cangahua, using the PPI endmember extraction algorithm applied to Landsat 8 OLI/TIRS multispectral images in the Ilaló volcano in order to jointly with a physicochemical characterization of the soil
- Obtaining an approximation of the surface occupied by cangahuas and know the state of the erosive process in order to show the real situation of this soils of this emblematic, protected area of Quito – Ecuador.

II. MATERIALS AND METHODS

A. Study Area

The Ilaló is a mountainous elevation made up of what was left after the eruption of a now-extinct volcano, which is located in the center of the Inter-Andean depression, southeast of the city of Quito, capital of Ecuador (Figure 1), whose slopes were eroded by glaciers [17].
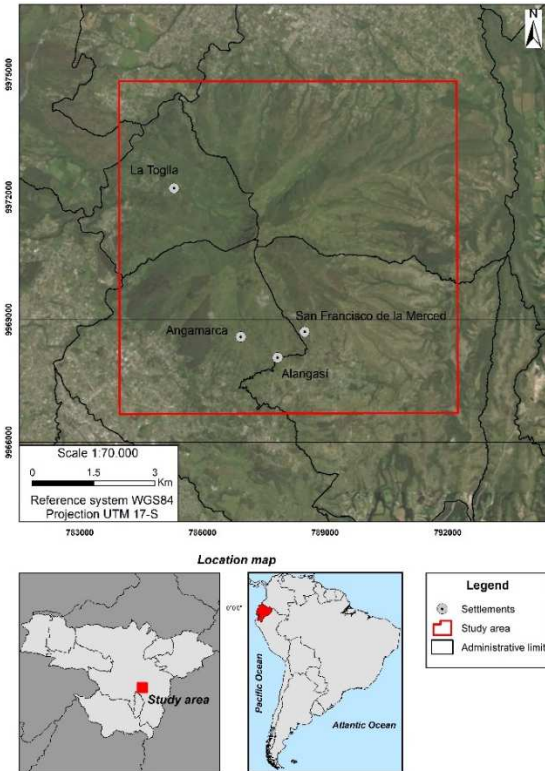

Fig. 1 Location map of the study area

The Ilaló volcano is part of the Metropolitan District of Quito; however, despite being a protected area, it presents an accelerated change in the existing vegetation cover, mainly due to indiscriminate logging. This problem, added to the steep slopes, the advance of the agricultural frontier, and poor planting practices by the inhabitants of the communities located on the slopes of the old volcano, have had an impact on the soil quality and have given way to the outcrop of one of the most common edaphological formations, cangahua (Figure 2), which in Quichua means "sterile hard land" [18]. It contributes significantly to the erosive processes of this region.

The cangahua is a geological formation of ryodacytic ash [19], originated by the partial diagenesis of the fine and hardened explosive volcanic material caused by pyroclastic falls. In Ecuador, cangahua can be found in the northern part of the Inter-Andean valley [20]. This area stands out for the serious soil erosion analyzed in the study and its history and unique geological features.

Fig. 2 Forest cover deforestation (A) and outcropping cangahuas in Ilaló volcano (B)

B. Radiometric and atmospheric correction

Landsat 8 OLI/TIRS images have certain advantages compared to their predecessors TM and ETM+, for example, this satellite takes approximately 725 images every day about, with three additional spectral bands (central wavelengths: 0.443 μm, 1.375 μm, 11.45 ± 0.555 μm), has a delay time of fewer than 8 hours after capture and, in addition, it allows to achieve better geometric and radiometric correction accuracies [21].

Before processing, it is necessary to make certain corrections to the image to avoid distortions or errors in the classification [8]. The Landsat 8 images have a geometric correction. However, radiometric correction is required to convert the image's digital numbers (DN) at apparent radiance values [9]. In the case of radiometric calibration, the radiance TOA (Top of Atmosphere) R_λ [W/(m². sr. μm)] is calculated by (1), with the digital numbers of the image to correct the influence of the solar zenith angle between the acquisition of the information. The value of the gain coefficients G_λ and compensation factor O_λ is obtained from the metadata.

$$R_\lambda = G_\lambda * DN + O_\lambda \qquad (1)$$

The satellite's due to the gas dispersion and aerosological absorption present in the atmosphere [2]. This bias is corrected utilizing an atmospheric calibration in TOA radiance, using the Fast Line-of-Sight Atmospheric Analysis of Spectral Hypercubes (FLAASH), a module based on MODTRAN 4, found in ENVI v.5.1 [22], with which the surface reflectance is obtained. The atmospheric parameters for atmospheric calibration are a function of the time and location of each image [23].

C. Minimum Noise Fraction (MNF)

Principal component analysis (PCA) presents the difficulty of not segregating adjacent noise in the dataset [24]. This problem is solved by applying a transformation MNF or also called cascading PCA [1]. Its most notable difference is that MNF considers noise within the data set, while PCA only considers the variations of each vector [25]. The noise value existing in the dataset is not always constant everywhere, but the variance of the noisy data is greater than the variance of the actual data, so the principal components obtained with MNF are better [1].

The transformation MNF serves to reduce dimensionality and eliminate noise in data [26]. The algorithm performs two principal component transformations; the first converts the noise covariance matrix into an identity matrix (whitening step) [27], thereby obtaining the mean for each band of the input image, statistics of the noise covariance, and statistics of the covariance of the bleached and rescaled input data [1], these are calculated using the exchange difference method [26]. The second is a standard transformation of the principal component of the noise bleached data set that maximizes the signal/noise ratio (SNR), with which the matrix of vectors and eigenvalues is obtained and the separation between SNR [22].

D. Pixel Purity Index (PPI)

The algorithm PPI is based on a convex geometry [28], where data vectors are defined with a minimum or maximum orthogonal projection towards a certain direction [1] (Figure 3).
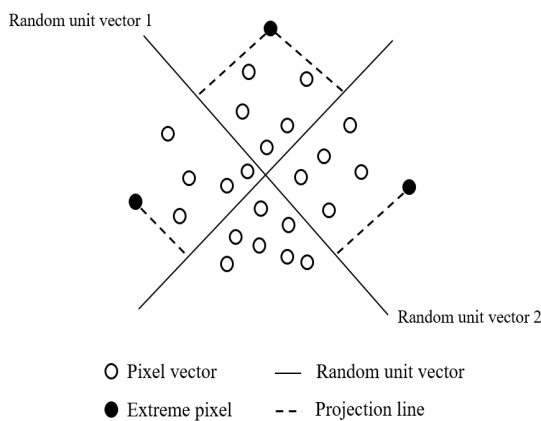

Fig. 3 PPI diagram. Source: Adapted de Xu et al., [29]

PPI acts on the MNF image with thousands of repetitions, where the number of times that a pixel was treated as extreme is indicated [27]. This algorithm iteratively works with projections that produce n-dimensional scatterplots in a random unit vector [22], where the extreme pixels are recorded in each projection and the total number that these were considered external [30]. The pixels that are furthest to the extreme are considered pure pixels and will be the ones that help determine the potential spectra of the image of the endmembers through spectral mixing [9]. Using a threshold value, the extreme pixels of the projected vector is defined. Figure 4 shows the iterations of PPI versus total pixels on the PPI graph. This threshold should be approximately two or three times that of the noise level in the data [22]. The PPI finds more extreme pixels; however, endmembers are less likely to be pure [1].
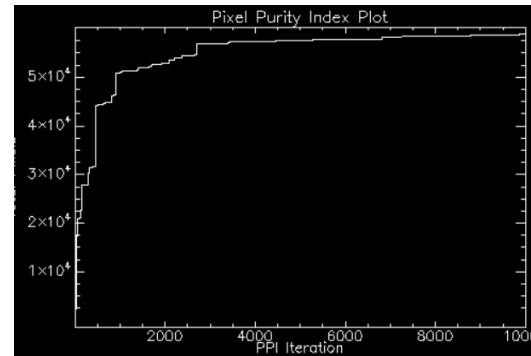

Fig. 4 PPI graph with the iterations for all pixels

E. n-Dimensional visualizer

The n-D (or n-Dimensional) viewer is a handy interactive tool for locating, identifying and matching spectral pure or unique pixels in the image [27]. Thus, it is possible to graph the image data in the spectral space, where the display's axes correspond to the images' bands [22]. n-D is commonly used with MNF data from a spatial subset of pure pixels obtained from PPI [31]. The PPI scatterplot makes it easier to select the purest pixels by rotating their axes.

F. Extraction of endmembers

In the extraction of the endmembers of the image, two methods were used: Spectral Angle Mapper (SAM) and Linear Spectral Unmixing (LSU). These two forms of endmember extraction are the most widely used in PPI; therefore, it was applied, and its subsequent results are compared.

SAM enables rapid classification mapping by calculating the spectral similarity between the image spectra and the referential reflectance spectra [22] (in this case, the pure spectral value of the object compared to the spectral library of endmembers obtained in the previous step). SAM is less sensitive to solar illumination errors because the angle between the two vectors is independent of the length of the vector [27]. It is calculated by (2) with the following equation [32]:

$$\theta = \text{Cos}^{-1}\left[\frac{\sum_{i=1}^{n} t_i * r_i}{\sqrt{\sum_{i=1}^{n} t_i^2 * \sum_{i=1}^{n} r_i^2}}\right] \qquad (2)$$

Where t and r are the sources and target spectra, respectively, i is the image band, and θ is the average angle. The angular difference is the output of the SAM function, measured in radians $(0 - \pi/2)$ [1]. It is important to note that if the spectral angle (SA) is slight, there is a similarity between t and r, and vice versa [22].

The LSU model is another method used for mixed pixel decomposition [33]. This can determine the abundance of endmembers of the image according to the spectral characteristics of the different surface coverages under study [34]. LSU is based on three assumptions: a) the reflectance of the pixels comes from a linear combination between the reflectance of the endmember and the portion of the area that the endmember occupies in the pixel, b) the endmembers are isolated, homogeneous, and do not have multiple dispersion, c) contiguous pixels do not affect the spectrum of a target pixel [9]. Equation (3) shows the model:

$$D_{Ni} = \sum_{j=1}^{p} m_{ij} * \alpha_j + e_i \qquad (3)$$

Where p is the number of endmembers, i represents the index of the band, mij is the reflectance of the endmember j in band i, αj is the proportion of the area that the endmember j occupies in a pixel, e_i is the error adjacent in band i.

G. Physical and chemical characterization of the soil

To carry out the measurement, soil samples were collected at a depth of approximately 15 cm in La Toglla, Alangasí, La Merced, and Angamarca communities, located on the slopes of the Ilaló volcano of parameters in the laboratory and relate the results to the mapping of cangahuas. The physical parameters were: humidity, bulk density (BD), relative density (RD), and porosity; this analysis was based on the Mexican regulations on fertility, salinity, and soil classification NOM-021-SEMARNAT-2000 [35].

On the other hand, the chemical parameters were pH, electrical conductivity (EC), organic matter (OM), potassium, nitrates, and phosphates, in soil/water extracts 1:1, 1:5, and 1:10. In the measurement of potassium, nitrates, and phosphates, an atomic absorption spectrometer was used according to the methodology of The Standard Methods given by the American Public Health Association (APHA) [36].

III. RESULTS AND DISCUSSION

With the help of the n-D visualizer, four endmembers were selected (Figure 5A) that correspond to the coverings of dispersed vegetation, the body of water, leafy vegetation, and bare soil. Regions of interest (ROI) obtained the selection of the pure pixels of each coverage that, as a whole, defined a spectral library, the same one that served as training for the classification of the different coverage in the study area.

The two methodologies used for the classification of coverage were based on the library previously obtained. The resulting spectral collection of endmembers is shown in Figure 5B, which corresponds to the spectral signature of the identified coverages (green: leafy vegetation, magenta: bare soil; yellow: scattered vegetation, blue: a body of water).

The spectral graph corresponds to the behavior of the electromagnetic spectrum of light reflected by the different covers on the earth's surface [37]. In Figure 5B, it is observed that the leafy vegetation presents a higher reflectance due to the presence of chlorophyll with a jump between the green and red band [38], contrary to what happens with scattered vegetation, which represents a mixture of low grass, soil and herbaceous vegetation, which is less reflective than bare soil [9]. The signature of the bare soil is very distinctive [39], which is a way to check the correct selection of the

endmembers and the spectral signature of water, whose behavior is not very reflective [2]. The result of mapping using SAM and LSU are shown in Figure 6.
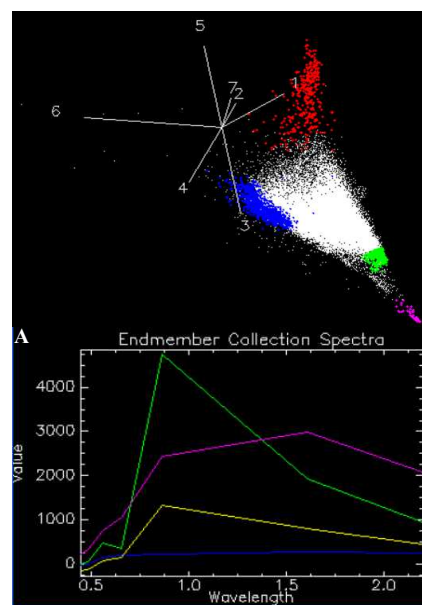

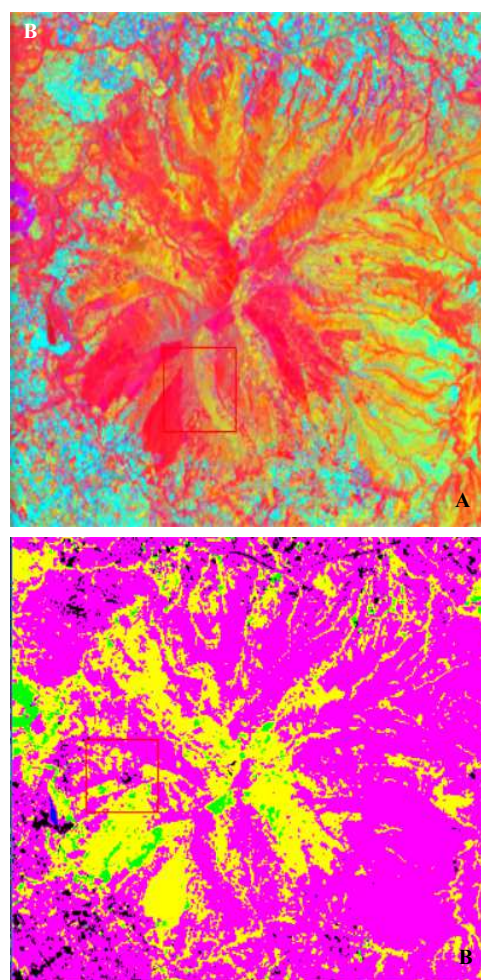Fig. 5 Selected members (A) and spectral collection of endmembers (B)

Fig. 6 Mapping obtained with LSU (A) and SAM (B)

In addition, based on the mapping methods of endmembers, a supervised classification was made from the vegetation

index: Normalized Difference Vegetation Index (NDVI), Soil-Adjusted Vegetation Index (SAVI), and Modified Soil-Adjusted Vegetation Index (MSAVI), in order to compare the results of the classification using PPI and the traditional methods of identification of coverage. The precision evaluation was carried out through a confusion matrix and the calculation of the Kappa coefficient to obtain the overall mapping precision and measure the degree of agreement of each classification, respectively. Table 1 shows the results of the tests applied.

TABLE I
ACCURACY OF THE HEDGE CLASSIFICATION METHODS

Method	Overall accuracy	Kappa Coefficient
LSU	91.271%	0.892
SAM	88.108%	0.854
NDVI	85.897%	0.781
SAVI	85.897%	0.781
MSAVI	86.538%	0.790

As seen in the values obtained from the confusion matrix and Kappa coefficient, coverage mapping using conventional object-oriented classification methods (based on vegetation index (NDVI) and soil (SAVI, MSAVI) respectively, was less accurate than that performed with the extraction of endmembers. Therefore, PPI presented a clear advantage over standard classifiers, proving itself to be a potent tool to discern the different objects of the territory, in this case, soils with cangahua. LSU was the method that reached the most agreement and precision.

Subsequent work in the field helped validate the effectiveness of the obtained result (LSU) in identifying the sites cataloged as discovered or with scattered vegetation, in which the presence of cangahua, mostly outcropping, could be confirmed (superficial). Although after the field visit, a high degree of erosion was visually evident, the interpretation of the physical and chemical parameters allowed characterizing and knowing the real state of the soil.

Physical parameters listed in Table 2 indicate low humidity content, which translates into poor water retention and consequently low oxygen availability. This result contrasts with the porosity percentage of around 45%, a value within the range for sandy-type soils, which goes from 35% to 50% and indicates an abundant runoff, and minimal water retention [40]. On the other hand, the average RD was 2.271 g/cm3, a value higher than the BD of all the samples, suggesting medium compaction of the soil [41].

TABLE II
PHYSICAL PARAMETERS OF THE SOIL WITH CANGAHUA

Sector	Humidity (%)	BD (g/cm^3)	RD (g/cm^3)	Porosity (%)
La Toglla	6.04%	1.136	2.097	45.83
La Merced	9.68%	1.250	2.248	44.39
Alangasí	8.46%	1.315	2.359	44.23
Angamarca	5.06%	1.280	2.380	46.08

The results of the chemical parameters shown in Table 3 indicate pH values within the range of 7.5 to 7.8, corresponding to alkaline soil. Most crops grow better if the soil pH is between 6.0 and 7.5 as the nutrients are readily available and in an appropriate balance. In alkaline soils, saturation and excess calcium prevent elements such as Iron from being absorbed by the plants [42].

TABLE III
CHEMICAL PARAMETERS OF THE SOIL WITH CANGAHUA IN THE STUDY AREA.

Sector	Soil extract	pH	EC (µS/cm)	OM (%)	Nitrates (ppm)	Phosphates (ppm)	Potassium (ppm)
La Toglla	1:1	7.66	0.873	0.00005958	6.60	0.23	0.99
	1:5	7.69	0.872	0.00028440	9.00	0.34	0.94
	1:10	7.66	0.881	0.00059220	15.00	0.27	1.20
La Merced	1:1	7.5	0.551	0.00005909	1.30	0.51	0.49
	1:5	7.8	0.475	0.00032555	5.00	0.35	0.41
	1:10	7.8	0.483	0.00031370	16.00	0.32	0.31
Alangasí	1:1	7.1	0.460	0.00000097	0.45	0.01	0.78
	1:5	7.6	0.470	0.00000625	6.00	0.15	0.76
	1:10	7.8	0.471	0.00001570	6.00	1.24	0.63
Angamarca	1:1	7.6	0.360	0.00000114	2.00	0.10	0.31
	1:5	7.8	0.370	0.00000100	17.50	0.28	0.11
	1:10	7.7	0.385	0.00004050	16.00	0.16	0.08

EC is correlated with soil properties that affect crop productivity (texture, cation exchange capacity, drainage conditions, organic matter, salinity, and subsoil characteristics) [43]. While each crop survives different ranges of conductivity depending on the type of salts, it can be said in a general way that: <750 µS/cm, none degree of restriction; 750-1500 µS/cm, slight to moderate degree of restriction; >1500 µS/cm, severe degree of restriction [44]. The electrical conductivity values measured in the sample extracts were very low, < 500 µS/cm. That is, they had a low amount of salts.

OM is useful for indirectly knowing soil fertility by improving the microstructure and having a high cation exchange capacity. The lack of OM reflects problems with the

soil structure resulting in the hardness of the soil and a limited water flow, this accompanies a decrease in fertility, and together they cause a general degradation of the soil [45]. In this case, the percentage of OM present in the samples is almost zero, indicating the soil's poverty and tendency to erosion.

The presence of nitrates, phosphates, and potassium is directly linked to the type of soil and the region where it is located. During the fieldwork, a large number of outcropping cangahua, typical of the Inter-Andean region, were observed; in addition, the low levels of nitrates, phosphates, and potassium found in the samples from the four communities (Table 3) agree with the expected levels in recently discovered cangahuas that have not received any type of qualification either for agriculture or naturally [45].

The results obtained from the physical and chemical analysis show poor soil and signs of erosive processes, in addition, it agrees with the characteristics of recently discovered cangahuas. This is related to the field visits and the mapping carried out, which showed the lack of vegetation cover and a large area of outcropping cangahua.

IV. CONCLUSION

The land surface coverage mapping in the study area showed greater precision by extracting endmembers with PPI than the traditional supervised classification that cannot discriminate the adjacent noise in each pixel of the image, enhancing PPI as an optimal technique for determining coverage in very heterogeneous areas. LSU showed a better fit than SAM for this case study from the two methodologies used in PPI. With an overall precision of 91.27% and 88.10%, a Kappa coefficient of 0.89 and 0.85 for the first and second, respectively, where LSU identified an area of approximately 806.85 ha of bare soil with cangahua.

The physical parameters analysis indicated that it is a moderately compacted soil with low humidity and a porosity typical of sandy-type soil. It can make water retention difficult and, in turn, reduces the available oxygen, added to the low content of OM found, an alkaline pH greater than 7.5, and the scarce presence of nutrients such as nitrates, phosphates, and potassium. It resulted in the soil present in the communities corresponds to poor, degraded soil, with a tendency to erosion. Such as mapping and sampling performed most of the soil in the study area is made up of outcropping cangahua, a situation that magnifies the erosive processes. Therefore, the recovery of the substrate and the habilitation of cangahuas in the Ilaló volcano is urgent to stop the deterioration.

REFERENCES

[1] S. Jasmine and V. Pattabiraman, "Improved pure pixel identification algorithms to determine the endmembers in hyperspectral images," *Comput. Electr. Eng.*, vol. 71, pp. 515–532, Oct. 2018.

[2] X. Wang *et al.*, "A robust Multi-Band Water Index (MBWI) for automated extraction of surface water from Landsat 8 OLI imagery," *Int. J. Appl. Earth Obs. Geoinf.*, vol. 68, pp. 73–91, Jun. 2018.

[3] N. Beisel, J. Callaham, N. Sng, D. Taylor, A. Paul, and R. Ferl, "Utilization of single-image normalized difference vegetation index (SI-NDVI) for early plant stress detection," *Appl. Plant Sci.*, vol. 6, no. 10, p. e01186, 2018.

[4] F. Kausar and M. Shahbaz, "Influence of strigolactone (GR24) as a seed treatment on growth, gas exchange and chlorophyll fluorescence of wheat under saline conditions," *Int. J. Agric. Biol.*, vol. 19, pp. 321–327, 2017.

[5] P. Towers, A. Strever, and C. Poblete, "Comparison of Vegetation Indices for Leaf Area Index Estimation in Vertical Shoot Positioned Vine Canopies with and without Grenbiule Hail-Protection Netting," *Remote Sens.*, vol. 11, no. 9, p. 1073, 2019.

[6] E. Özelkan, "Water Body Detection Analysis Using NDWI Indices Derived from Landsat-8 OLI," *Polish J. Environ. Stud.*, vol. 29, no. 2, pp. 1759–1769, 2020.

[7] I. Palacios, "Generación de un modelo de crecimiento tendencial urbano de la ciudad de Macas (Ecuador) al año 2030, mediante técnicas de modelación espacial multivariable," Universitat de Barcelona, Barcelona, 2020.

[8] M. Cepeda, I. Palacios, A. Tierra, and E. Kirby, "Multiresolution analysis in the visible spectrum of Landsat-TM images through Wavelet Transform," *Geogr. Tech.*, vol. 13, no. 1, pp. 20–29, 2018.

[9] J. Wu, Z. Gao, Q. Liu, Z. Li, and B. Zhong, "Methods for sandy land detection based on multispectral remote sensing data," *Geoderma*, vol. 316, pp. 89–99, Apr. 2018.

[10] S. Kaur *et al.*, "Mixed Pixel Decomposition Based on Extended Fuzzy Clustering for Single Spectral Value Remote Sensing Images," *J. Indian Soc. Remote Sens.*, vol. 47, pp. 427–437, 2019.

[11] W. Luo, L. Gao, R. Zhang, A. Marinoni, and B. Zhang, "Bilinear normal mixing model for spectral unmixing," *IET Image Process.*, vol. 13, no. 2, pp. 344–354, 2019.

[12] D. Nalawade *et al.*, "Hyperspectral Remote Sensing Image Analysis with SMACC and PPI Algorithms for Endmember Extraction," in *Recent Trends in Image Processing and Pattern Recognition. RTIP2R 2018*, 2019, pp. 319–328.

[13] A. Sharifi and M. Hosseingholizadeh, "Validation of Extracted Endmembers from Hyperspectral Images," *Int. Arch. Photogramm. Remote Sens. Spat. Inf. Sci.*, vol. XLII-4/W18, pp. 989–992, 2019.

[14] W. Jiménez, V. Loayza, and E. Metzler, "Mapping cangahua in Ecuador using remote sensing," *Siembra*, vol. 5, no. 1, pp. 38–50, 2018.

[15] I. Palacios, S. Castro, and F. Rodríguez, "Almacenamiento de carbono como servicio ambiental en tres reservas naturales del Ecuador," *Rev. Geoespacial*, vol. 16, no. 1, pp. 1–14, 2019.

[16] I. Palacios, D. Ushiña, and D. Carrera, "Identificación de Cangahuas para su recuperación mediante estudio multicriterio y constatación in situ en comunas del volcán Ilaló," in *Congreso de Ciencia y Tecnología ESPE*, Jun. 2018, vol. 13, no. 1, pp. 9–12.

[17] D. Carrera, J. Carrera, T. Braun, Z. Zhao, J. Gómez, and J. Carabalí, "Fog Harvesting and IoT based Environment Monitoring System at the Ilalo volcano in Ecuador," *Int. J. Adv. Sci. Eng. Inf. Technol.*, vol. 10, no. 1, pp. 407–412, 2020.

[18] J. Espinosa and M. J., "Agricultural Land Use," in *The Soils of Ecuador. World Soils Book Series*, Cham: Springer, 2018, pp. 151–162.

[19] P. Podwojewski and N. Germain, "Evolution of the soil structure in a deep tilled hardened volcanic ashsoil (Cangahua) in Ecuador," *Eur. J. Soil Sci.*, vol. 39, pp. 39–51, 2005.

[20] I. Palacios, D. Ushiña, and D. Carrera, "Técnicas SIG para recuperación de suelos cangahuosos, con fines de agricultura comunitaria en el Ilaló," *Cienc. del Suelo*, vol. 38, no. 2, pp. 295–309, 2020.

[21] F. Chen, S. Yang, K. Yin, and P. Chan, "Challenges to quantitative applications of Landsat observations for the urban thermal environment," *J. Environ. Sci.*, vol. 59, pp. 80–88, 2017.

[22] G. Krishna, R. Sahoo, S. Pradhan, T. Ahmad, and P. Sahoo, "Hyperspectral satellite data analysis for pure pixels extraction and evaluation of advanced classifier algorithms for LULC classification," *Earth Sci. Informatics*, vol. 11, no. 2, pp. 159–170, Jun. 2017.

[23] R. Chastain, I. Housman, J. Goldstein, M. Finco, and K. Tenneson, "Empirical cross sensor comparison of Sentinel-2A and 2B MSI, Landsat-8 OLI, and Landsat-7 ETM+ top of atmosphere spectral characteristics over the conterminous United States," *Remote Sens. Environ.*, vol. 221, pp. 274–285, 2019.

[24] T. Bangira, S. Alfieri, M. Menenti, A. Van Niekerk, and Z. Vekerdy, "A Spectral Unmixing Method with Ensemble Estimation of Endmembers: Application to Flood Mapping in the Caprivi Floodplain," *Remote Sens.*, vol. 9, no. 10, p. 1013, 2017.

[25] M. Elkholy, M. Mostafa, H. Ebied, and M. Tolba, "Hyperspectral unmixing using deep convolutional autoencoder," *Int. J. Remote Sens.*, vol. 41, no. 12, pp. 4799–4819, 2020.

[26] F. Fen, W. Li, Q. Du, and B. Zhang, "Dimensionality Reduction of Hyperspectral Image with Graph-Based Discriminant Analysis Considering Spectral Similarity," *Remote Sens.*, vol. 9, no. 4, p. 323, 2017.

[27] H. Suryoprayogo, F. Ramdani, and F. Utaminingrum, "Mapping Paddy Growth Stage Based-on Hyperspectral EO-1 Hyperion using Pixel Purity Index Endmember Extraction Algorithm," *J. Telecommun. Electron. Comput. Eng.*, vol. 10, no. 1–6, pp. 47–54, 2018.

[28] D. Shah, T. Zaveri, and Y. Trivedi, "Convex Polygon Maximization-Based Hyperspectral Endmember Extraction Algorithm," *J. Indian Soc. Remote Sens.*, vol. 49, pp. 419–432, 2021.

[29] N. Xu, Y. HU, B. Lei, C. Zhang, D. Wang, and T. Shi, "Automated mineral information extraction based on PPI algorithm for hyperspectral imagery," *Sci. Surving Mapp.*, vol. 38, no. 1, pp. 138–141, 2013.

[30] S. Jasmine and V. Pattabiraman, "Performance Analysis of Statistical-Based Pixel Purity Index Algorithms for Endmember Extraction in Hyperspectral Imagery," in *Advances in Intelligent Systems and Computing*, 2018, pp. 157–167.

[31] M. Solankar, H. Gite, R. Dhumal, R. Surase, D. Nalawade, and K. Kale, "Recent Advances and Challenges in Automatic Hyperspectral Endmember Extraction," in *Proceedings of 2nd International Conference on Communication, Computing and Networking*, 2018, pp. 445–455.

[32] D. Renza, E. Martinez, I. Molina, and D. Ballesteros, "Unsupervised change detection in a particular vegetation land cover type using spectral angle mapper," *Adv. Sp. Res.*, vol. 59, no. 8, pp. 2019–2031, 2017.

[33] D. Gudex, J. Pontius, and A. Adams, "Enhanced forest cover mapping using spectral unmixing an object-based classification of multi-temporal Landsat imagery," *Remote Sens. Environ.*, vol. 196, pp. 193–204, 2017.

[34] Y. Qu *et al.*, "Hyperspectral Anomaly Detection Through Spectral Unmixing and Dictionary-Based Low-Rank Decomposition," in *IEEE Transactions on Geoscience and Remote Sensing*, 2018, pp. 4391–4405.

[35] Secretaria de Medio Ambiente y Recursos Naturales, *NOM-021-SEMARNAT-2000: Norma Oficial Mexicana que establece las especificaciones de fertilidad, salinidad y clasificación de suelos, estudio, muestreo y análisis*. México: Diario Oficial de la Federación, 2002.

[36] APHA, *Standard Methods for the examination of water and wastewater*. Washington: Publication office American Public Health Association, 1995.

[37] E. Woźniak, R. Gabryszewski, and D. Dziob, "Remote sensing and electromagnetic wave behaviour to measure vegetation phenology with physics," *Phys. Educ.*, vol. 55, no. 4, p. 045012, 2020.

[38] P. Morley, A. Jump, M. West, and D. Donoghue, "Spectral response of chlorophyll content during leaf senescence in European beech trees," *Environ. Res. Commun.*, vol. 2, no. 7, p. 071002, 2020.

[39] A. Rasul *et al.*, "Applying built-up and bare-soil indices from Landsat 8 to cities in dry climates," *Land*, vol. 7, no. 3, pp. 81–94, Sep. 2018.

[40] J. Jones, *Laboratory guide for conducting soil tests and plant analysis*. New York: CRC Press, 2001.

[41] D. Carrera *et al.*, "Dynamic model and geospatial study for soil loss in the ancestral community of La Toglla," in *18th LACCEI International Multi-Conference for Engineering, Education, and Technology*, 2020, pp. 1–9.

[42] D. Horneck, D. Sullivan, J. Owen, and J. Hart, *Soil Test Interpretation Guide*. Oregon: Oregon State University, 2011.

[43] P. Hazelton and B. Murphy, *Interpreting Soil Test Results: What Do All the Numbers Mean?*, 3rd ed. Clayton South: CSIRO Publishing, 2016.

[44] M. Zaman, S. Shahid, and L. Heng, "Irrigation Water Quality," in *Guideline for Salinity Assessment, Mitigation and Adaptation Using Nuclear and Related Techniques*, Cham: Springer, 2018, pp. 113–131.

[45] C. Ortega and S. Calderón, "Evaluación del potencial productivo de Cangahuas de diferentes edades de habilitación con dos especies forrajeras (Lolium multiflorum y Trifolium pratense)," Universidad Central del Ecuador, Quito, 2015.